

## Article

# MgF<sub>2</sub>-Modified Hydrotalcite-Derived Composites Supported Pt-In Catalysts for Isobutane Direct Dehydrogenation

Zhen Song, Jiameng Wang, Fanji Liu, Xiqing Zhang, Énio Matusse and Lihong Zhang \*

Department of Catalysis Science and Technology and Tianjin Key Laboratory of Applied Catalysis Science & Technology, School of Chemical Engineering and Technology, Tianjin University, Tianjin 300350, China; songzhens12345@163.com (Z.S.); wangjiameng0216@163.com (J.W.); lfj19961018@163.com (F.L.); zhangxiqing1997@163.com (X.Z.); enio\_matusse@outlook.com (É.M.)

\* Correspondence: zlh\_224@tju.edu.cn; Tel.: +86-150-2225-5828

**Abstract:** Here, a simple method was developed to prepare an MgF<sub>2</sub>-modified hydrotalcite-derived composite, which was used as support for the Pt-In catalyst for isobutane direct dehydrogenation. The catalysts, composites, and their precursors were characterized by numerous characterization techniques. The results provided evidence for the MgF<sub>2</sub> promoter effect on the physical–chemical properties and dehydrogenation performance of the supported Pt-In catalysts. The catalyst with MgF<sub>2</sub> shows exceptional isobutene selectivity that can be stabilized at 95%, and the conversion increases from 50% to 58% during the reaction process. Moreover, the existence of MgF<sub>2</sub> plays an important role in the resistance to coke formation and Pt sintering by improving the Pt dispersion, inhibiting the reduction of the In<sup>3+</sup> species, and adjusting the acidity of the catalyst.

**Keywords:** isobutane dehydrogenation; MgF<sub>2</sub> promoter; hydrotalcite-derived composites; supported Pt-In catalysts



**Citation:** Song, Z.; Wang, J.; Liu, F.; Zhang, X.; Matusse, É.; Zhang, L. MgF<sub>2</sub>-Modified Hydrotalcite-Derived Composites Supported Pt-In Catalysts for Isobutane Direct Dehydrogenation. *Catalysts* **2021**, *11*, 478. <https://doi.org/10.3390/catal11040478>

Academic Editors: Juan Antonio Cecilia and Carmen Pilar Jiménez Gómez

Received: 16 March 2021  
Accepted: 6 April 2021  
Published: 8 April 2021

**Publisher's Note:** MDPI stays neutral with regard to jurisdictional claims in published maps and institutional affiliations.



**Copyright:** © 2021 by the authors. Licensee MDPI, Basel, Switzerland. This article is an open access article distributed under the terms and conditions of the Creative Commons Attribution (CC BY) license (<https://creativecommons.org/licenses/by/4.0/>).

## 1. Introduction

In recent years, the sharp increase in the global demand for olefins is driven by the rapid growth in the demand for downstream products in the world [1]. Additionally, isobutene, as a raw material of butyl rubber [2], polyisobutene, and other downstream products, has attracted a lot of attention. At present, the direct dehydrogenation of isobutane represents an environmentally friendly and cost-effective preparation method [3,4].

It is well known that Pt is the most effective active metal for dehydrogenation of light alkanes, but it is easy to sinter and has relatively poor stability [5,6]. Some metallic promoters, such as Sn [7–9], In [10–13], Cu [14], Zn [15,16], Ga [17,18], K [19,20], or Ge [21,22], are usually used to enhance the interaction with Pt from the electronic and geometric aspects so as to resist coke deposition, suppress Pt sintering, and improve the catalytic performance. In addition, the non-metallic promoters, involving element B [23], F [24,25], Cl [26], and P [27], are usually applied to adjust the acid sites and promote the dispersion of active sites on the surface of catalysts. In general, these promoters can not only modify the surrounding environment of the Pt active sites of catalyst, but also adjust some properties of the supports.

The support materials can also influence the catalytic performance, and a lot of studies have been conducted on the support materials, such as Al<sub>2</sub>O<sub>3</sub> [9,28,29], MgO [30], SiO<sub>2</sub> [27,31], ZrO<sub>2</sub> [15,23,32], and spinel ZnAl<sub>2</sub>O<sub>4</sub> [7,33,34], for isobutane dehydrogenation catalysts. Now, the focus has been switched to calcined hydrotalcite or hydrotalcite-like (HT) composites, which have been used in direct dehydrogenation of propane and have good performance compared to other supports [10–12]. Calcined hydrotalcite or hydrotalcite-like (HT) materials are the typical composite metal oxides [35–37]. These have suitable surface acidic characteristics and high specific surface area, which is conducive to

the adsorption of alkanes and the desorption of alkenes and enhances Pt particle dispersion. Among recent studies, some have reported that PtIn catalysts with calcined MgAl hydrotalcite-like as supports compared to spinel as supports exhibited high activity and better selectivity in propane dehydrogenation reaction processes [12]; others reported that Pt-based catalysts substituting Al with In cation on calcined hydrotalcite-like supports also displayed excellent performance of alkanes dehydrogenation [38]. In particular, as far as we know, no report discusses the catalytic performance of Pt-In catalysts supported on MgF<sub>2</sub>-modified calcined hydrotalcite-like carriers in isobutane direct dehydrogenation.

In our work, we successfully synthesized the MgF<sub>2</sub>-modified HT-derived composite supported Pt-In catalyst, which exhibited great catalytic performance. The synthesis process includes hydrothermal, alkali-etching, calcination, and impregnation of Pt and In precursors, together with calcination and reduction pretreatment. To discuss the relationships of the isobutane dehydrogenation performance of catalysts with the physicochemical properties, numerous characterization techniques were employed for the as-prepared and spent catalysts.

## 2. Results and Discussion

### 2.1. Characterization of Composite Supports and Catalysts

#### 2.1.1. The X-Ray Diffraction (XRD)

Figure 1A,B shows the X-ray diffraction (XRD) patterns of the support composites and corresponding supported Pt-In catalysts with calcining and reducing treatment. The characteristic peaks of HT phase (JCPDS file No. 51-1525) are observed in the composites (Figure 1A). Obviously, the HT phase is the only crystalline phase for the reference HT composite. At the same time, an additional MgF<sub>2</sub> phase (JCPDS file No. 41-1443) can be detected in the HT-MgF<sub>2</sub> composite, followed by the decrease in HT diffraction peak intensity. After calcination and reduction (see Figure 1B), the diffraction peaks of the periclase MgO phase (JCPDS file No. 45-0946) appear. However, the diffraction peaks of the Pt and In species cannot be found. This arises from their small particle size and/or low concentration below XRD detection limit, indicating that Pt and In particles are well dispersed on the supports.

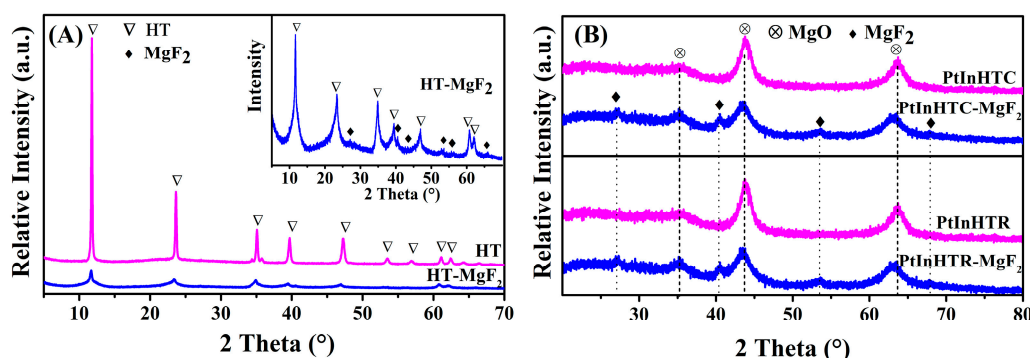


**Figure 1.** X-ray diffraction (XRD) patterns of (A) the support composites and (B) the calcined and reduced catalysts.

#### 2.1.2. N<sub>2</sub>-Adsorption–Desorption Isotherms

The textural properties of the catalysts were characterized by a low-temperature N<sub>2</sub> adsorption–desorption technique, and the results are depicted in Figure 2A,B. As shown in Figure 2A, the isotherms exhibit the type IV curves with the H2 hysteresis loops indicating the characteristics of the hierarchical mesoporous structure. The corresponding pore size distributions are broad and mainly concentrated in the range of 3–30 nm, further confirming the hierarchical mesoporous feature. Compared with the textural properties of PtInHTC, PtInHTC-MgF<sub>2</sub> exhibits an increase in S<sub>BET</sub> of 216 m<sup>2</sup>·g<sup>-1</sup>, D<sub>p</sub> of 4.9 and 12.3 nm and V<sub>p</sub>. Additionally, the S<sub>BET</sub> of PtInHTC-MgF<sub>2</sub> is higher than that of the previous

dehydrogenation catalysts [13,38,39]. This means that the pore channel of PtInHTC-MgF<sub>2</sub> can provide more surface and space for adsorption and reaction of isobutane.

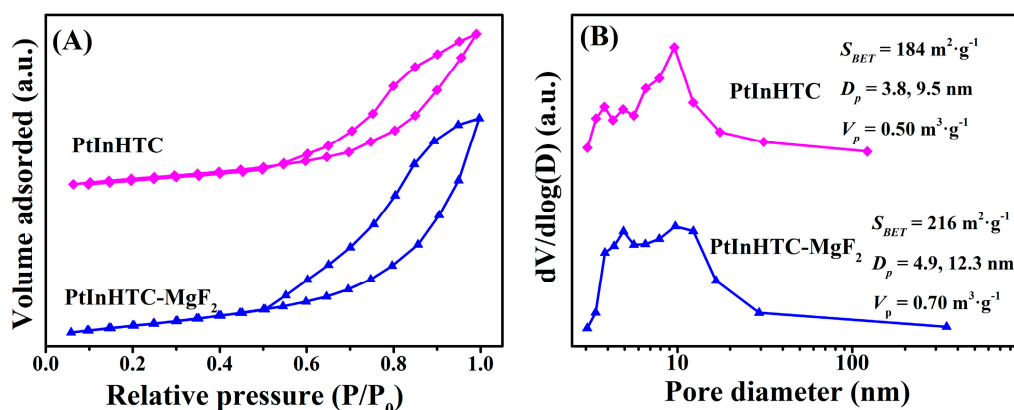


**Figure 2.** (A) Low temperature N<sub>2</sub> adsorption–desorption isotherms, (B) pore size distributions curves, and textural data of the calcined catalysts, involving BET special surface area ( $S_{BET}$ ), the most probable pore size determined by the BJH method ( $D_p$ ), and total pore volume ( $V_p$ ).

### 2.1.3. The Scanning Electron Microscopy (SEM) and the Transmission Electron Microscopy (TEM)

The morphologies of calcined catalysts are described by SEM images in Figure 3. Overall, the typical mesoporous morphology can be found for these composites. The calcined sample PtInHTC without MgF<sub>2</sub> mainly presents the large block mass particles [11]. The catalyst PtInHTC-MgF<sub>2</sub> shows that the abundant well-defined triangular pore channels are constructed by intersecting nanosheets. This means that the MgF<sub>2</sub> plays a key role in tuning the morphology and pore structure of catalysts. The main reason is that the presence of F<sup>-</sup> anions can activate the substrates to liberate more metal ions for nucleation and growth to obtain interconnected nanosheets in the synthesis process [40]. Figure 3C–F gives TEM images and particle size distribution (PSD) of the reduced catalysts. Their PSD are narrow, and the Pt (111) plan from Pt particles can be found on the reduced catalysts according to the lattice spacing of 0.226 nm, although there is no peak of metal Pt in the XRD phase (Figure 1B). These indicate the metal particles are well dispersed on these catalysts. It is important to point out that the average particle size decreases from 1.3 nm of PtInHTR to 1.2 nm of PtInHTR-MgF<sub>2</sub>, with a simultaneous narrowing of PSD. This can be attributed to the additional dispersion effect of MgF<sub>2</sub> on active metals. The small size of active metals is more favorable for the dehydrogenation reaction because the small active metals are less active for cracking reaction and deep dehydrogenation [41].

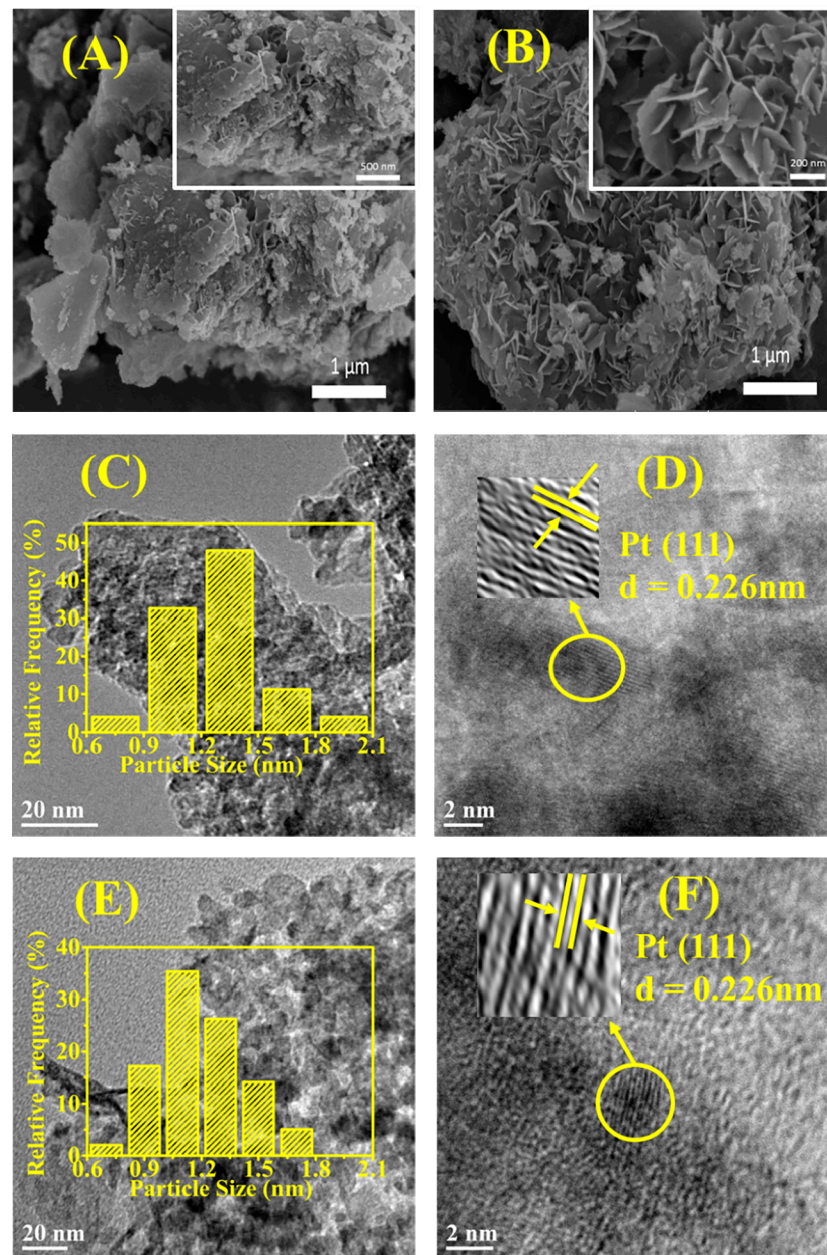


**Figure 3.** SEM images of PtInHTC (A) and PtInHTC-MgF<sub>2</sub> (B), TEM micrographs of catalysts PtInHTC (C,D), and PtInHTC-MgF<sub>2</sub> (E,F).

#### 2.1.4. The Temperature-Programmed Reduction (H<sub>2</sub>-TPR)

The H<sub>2</sub>-TPR results in Figure 4 show the reducibility of catalysts PtInHTC and PtInHTC-MgF<sub>2</sub>. It can be clearly seen that the catalyst PtInHTC exhibits a wide reduction peak with the maximum value at 466 °C (peak I) and shoulder peak at 560 °C (peak II), while the three relative separated peaks are mainly at 460 °C (peak I), 550 °C (peak II), and 634 °C (peak III) for catalyst PtInHTC-MgF<sub>2</sub>. According to the previous literature [12,42,43], peak I is attributed to the reduction of PtO<sub>2</sub>, and peak II can be related to the co-reduction of the Pt and In species. The formation of the peak III may be due to the removal of a small amount of surface hydroxyl. In addition, it can be found that the lower reduction temperature of peak I and peak II can be obtained for the catalyst PtInHTC-MgF<sub>2</sub>. This indicates that the formation of MgF<sub>2</sub> can reduce the reduction temperature of the Pt species to a certain extent. In other words, the weaker interaction between the Pt species and

supports can be achieved when the  $\text{MgF}_2$  species modified the supports. Additionally, it can be seen that the Pt species can be reduced before  $600\text{ }^\circ\text{C}$  for two catalysts.

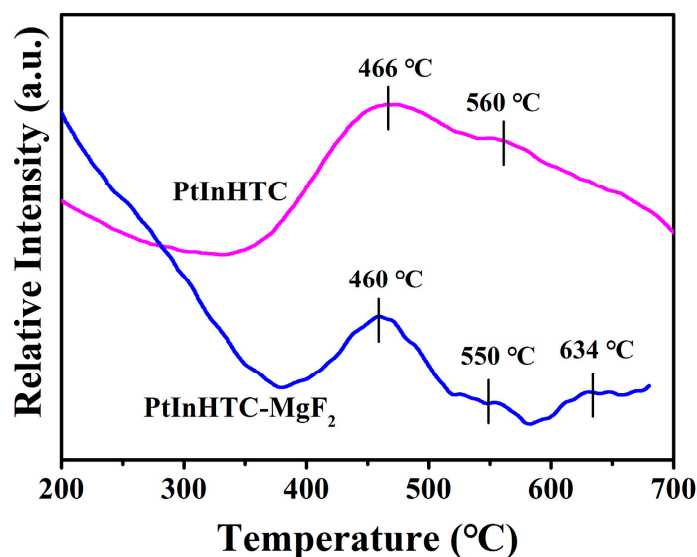


Figure 4.  $\text{H}_2$ -TPR profiles of the catalysts.

#### 2.1.5. X-Ray Photoelectron Spectroscopy (XPS)

The surface elemental compositions and chemical states of In, Mg, and F elements on the reduced catalysts were analyzed using X-ray photoelectron spectroscopy (XPS), and the XPS spectra of whole survey, In 3d, Mg 1s, and F 1s regions are shown in Figure 5, with a summary of the binding energy (BE) and ratio of  $\text{In}^{3+}/\text{In}^0$  for the samples in Table 1.

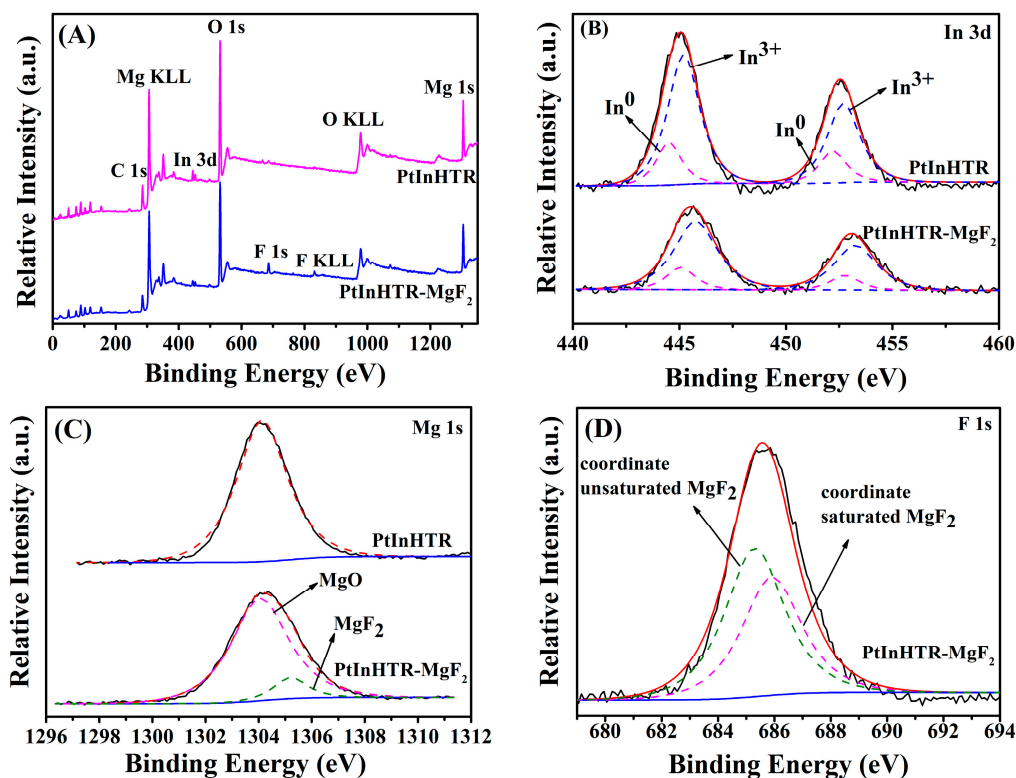


Figure 5. X-ray photoelectron spectroscopy (XPS) spectrum of (A) the whole survey, (B) In 3d, (C) Mg 1s, and (D) F 1s for the reduced catalysts.

**Table 1.** XPS results of the In 3d regions for the reduced catalysts.

Samples	Binding Energy (eV)				In <sup>3+</sup> /In <sup>0</sup> <sup>a</sup>
	In 3d <sub>5/2</sub>		In 3d <sub>3/2</sub>		
	In <sup>0</sup>	In <sup>3+</sup>	In <sup>0</sup>	In <sup>3+</sup>	
PtInHTR	444.5	445.2	452.2	452.7	3.5
PtInHTR-MgF <sub>2</sub>	444.5	445.2	452.2	452.7	4.2

<sup>a</sup> Calculated from the corresponding fitting peak area.

In Figure 5A, it can be seen that the F element is exactly detectable in PtInHTR-MgF<sub>2</sub>, compared with the sample PtInHTR. According to the results of XRD above, this further demonstrates the existence of MgF<sub>2</sub> on PtInHTR-MgF<sub>2</sub>. To explore the metal–support interaction in depth, the XPS spectra are mainly focused on the In 3d regions instead of the Pt 4f regions owing to the overlapping of the Pt 4f and Al 2p region peaks [44]. As shown in Figure 5B, the broad In 3d peak in the range of 440–460 eV can be deconvoluted into four peaks, which refer to two In species on the surface of PtInHTR-MgF<sub>2</sub>. The low BE value is attributed to the zero-valent In (In<sup>0</sup>), and the high BE is ascribed to the oxidation state of the surface In species (In<sup>3+</sup>). As listed in Table 1, the ratio of In<sup>3+</sup>/In<sup>0</sup> of PtInHTR-MgF<sub>2</sub> is higher than that of PtInHTR, indicating that the presence of MgF<sub>2</sub> can inhibit the reduction of In<sup>3+</sup> ions on the surface to avoid the formation of a PtIn alloy. Compared with PtInHTR and PtInHTR-MgF<sub>2</sub>, the same BE values for the different In species indicate that there is no electron transfer between the In species and MgF<sub>2</sub>. Accordingly, it can be deduced that the smaller amount of In<sup>0</sup> species should be due to the coverage of MgF<sub>2</sub> resulting in the difficult reduction of In<sup>3+</sup> species. Usually, it is proposed that the In<sup>3+</sup> species are favorable to dehydrogenation reaction, in view of the blockage of the active Pt sites by the In<sup>0</sup> species [10,13,45].

Then, Figure 5C illustrates the Mg 1s XPS spectra of the samples, and it can be observed that Mg species present in two chemical states. The peaks appearing at BE of 1304.1 eV and 1305.2 eV can be attributed to MgO and MgF<sub>2</sub> species in the reduced catalysts, respectively [46]. Moreover, according to the deconvolution of the spectra of F 1s (in Figure 5D), we can see two relevant fitted peaks, representing two different coordination states of the F species. The peak of F 1s at 686.0 eV comes from the saturated MgF<sub>2</sub>, and the peak with BE of 685.4 eV is attributed to F bound to under-coordinated Mg, namely, four- and five-fold coordinated, which is responsible for the Lewis acid sites [47]. Usually, the small MgF<sub>2</sub> particles are deemed to be the reason of the formation of the under-coordinated Mg and even weak acid sites [47]. However, the weak acid sites are favorable for coking-resistance in the dehydrogenation reaction. Therefore, it is reasonable to conclude that the formation of MgF<sub>2</sub>, especially the under-coordinated Mg species in MgF<sub>2</sub>, significantly affects the acidity and stability of catalysts and facilitates the resistance to coking and sintering.

## 2.2. Catalytic Dehydrogenation Performance of Catalysts

Figure 6 depicts the isobutane conversion, isobutene yield, and selectivity of isobutene and by-product methane over the reduced catalysts in the isobutane dehydrogenation reaction for 9 h. As can be seen from Figure 6A, the catalysts PtInHTR and PtInHTR-MgF<sub>2</sub> exhibit a rapid loss in conversion during the first 30 min and then attain a period of stable conversion throughout the dehydrogenation test. In detail, the catalyst PtInHTR gives the lowest conversion, while the conversion of PtInHTR-MgF<sub>2</sub> increases from 50% to 58% within 9 h. That is to say, the formation of MgF<sub>2</sub> really enhances the activity of the catalysts. It can be assigned to the special pore channels and surface features. From Figure 6B, it can be found that the isobutene selectivity of the catalyst PtInHTR-MgF<sub>2</sub> can be stabilized at 95% during the reaction process. Correspondingly, the catalyst PtInHTR exhibits declining isobutene selectivity. In addition, the selectivity of by-product methane is less than 5% and much lower than the corresponding isobutene selectivity. In particular, for catalyst PtInHTR-MgF<sub>2</sub> the by-product methane is almost completely inhibited during the reaction.

This indicates that the  $\text{MgF}_2$ -modification can inhibit the cracking reaction and improve the selectivity and stability of catalysts. Additionally, it is clear that the isobutene yield of  $\text{PtInHTR-MgF}_2$  is no less than 55% and is much higher than that of  $\text{PtInHTR}$ . The excellent catalytic dehydrogenation performance is closely related to the properties of the active species, promoters, and supports. The small size of Pt particles [48], stable  $\text{In}_2\text{O}_3$  state [10,45], and suitable acidic properties of the supports [49] on catalysts can greatly improve the activity and selectivity of the catalyst. According to the TEM and XPS analysis above,  $\text{PtInHTR-MgF}_2$  has a small active metal particle size, a stable chemical state of the  $\text{In}^{3+}$  species, and abundant weak acid sites, which are responsible for resistance to coking and sintering. Therefore,  $\text{PtInHTR-MgF}_2$  exhibited high activity and stable selectivity.

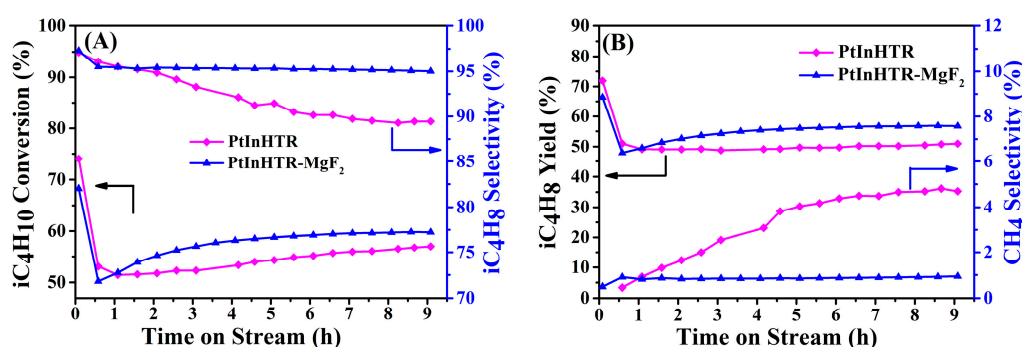


**Figure 6.** (A) Isobutane conversion and isobutene selectivity, (B) isobutene yield and by-product methane selectivity as functions of time. (Reaction conditions: 600 °C, 1 atm,  $\text{H}_2$ : $\text{iC}_4\text{H}_{10}$  = 1:1 (molar ratio),  $\text{WHSV}(\text{iC}_4\text{H}_{10}) = 3 \text{ h}^{-1}$ ,  $m_{\text{cat}} = 0.5 \text{ g}$ ).

In view of the superior dehydrogenation performance of  $\text{PtInHTR-MgF}_2$ , the detailed information compared with previously reported catalysts is collected in Table 2. In terms of conversion and selectivity, it demonstrates that the investigation of the catalyst  $\text{PtInHTR-MgF}_2$  is meaningful.

**Table 2.** Comparison of catalytic performance of various catalysts in isobutane dehydrogenation <sup>a</sup>.

Catalysts	Pt Contents (wt%)	WHSV ( $\text{h}^{-1}$ )	Isobutane Conversion (%) <sup>b</sup>	Isobutene Selectivity (%) <sup>b</sup>	References
$\text{PtInHTR-MgF}_2$	0.5	3	50–58	96–95	Present work
$\text{InPtSn/ZnAl}_2\text{O}_4$	0.4	4	54–38	94–96	[33]
$\text{PtNi/LaFeO}_3/\text{SiO}_2$	0.3	3	39–39	84–91	[39]
$\text{PtSnKMg/Al}_2\text{O}_3$	0.5	2	34–29	80–95	[50]
$\text{PtSnKZn/Al}_2\text{O}_3$	0.5	2	36–32	96–96	[51]
$\text{PtSnNa/ZSM-5}$	0.5	2.5	52–52	84–84	[52]

<sup>a</sup> From the considered articles, only the best catalytic performance is indexed. <sup>b</sup> Two data are recorded from the initial and the end stage, respectively.

### 2.3. Characterization of the Spent Catalysts

#### 2.3.1. Thermogravimetric Analysis (TG-DTA) and the X-ray Diffraction (XRD)

According to the TG curves in Figure 7A, the total mass losses of  $\text{PtInHTU}$  and  $\text{PtInHTU-MgF}_2$  are 60% and 17%, respectively. As expected, the coke deposition can be suppressed by forming  $\text{MgF}_2$  micro-crystals. The positive anti-coking ability is mainly related to the small active metals particles and weak acid sites supplied by  $\text{MgF}_2$  nanoparticles over  $\text{PtInHTR-MgF}_2$ . From the differential thermal analysis(DTA) peaks of the spent  $\text{PtInHTU}$ , it can be determined that there are two successive coke combustion regions, representing two different coke deposits. The small DTA peak at the low temperature range is assigned to the amorphous coke, while the big peak at a high temperature of 570 °C corresponds to the formation of serious graphitized coke [53]. Interestingly, only a small DTA peak, resulting from the combustion of amorphous coke, can be detected

for PtInHTU-MgF<sub>2</sub>. This suggests that it is more difficult for the active metal sites on PtInHTU-MgF<sub>2</sub> to be fully covered by the coke deposits and easier to be regenerated than those on PtInHTU. Additionally, from the XRD patterns shown in Figure 7B, the diffraction peaks of carbon at 2θ of 26° can be detected for the PtInHTU catalyst, but it is not detected on the PtInHTU-MgF<sub>2</sub> catalyst. This explains that there is a large amount of carbon on the catalyst PtInHTU catalyst, which is also consistent with the TG results.

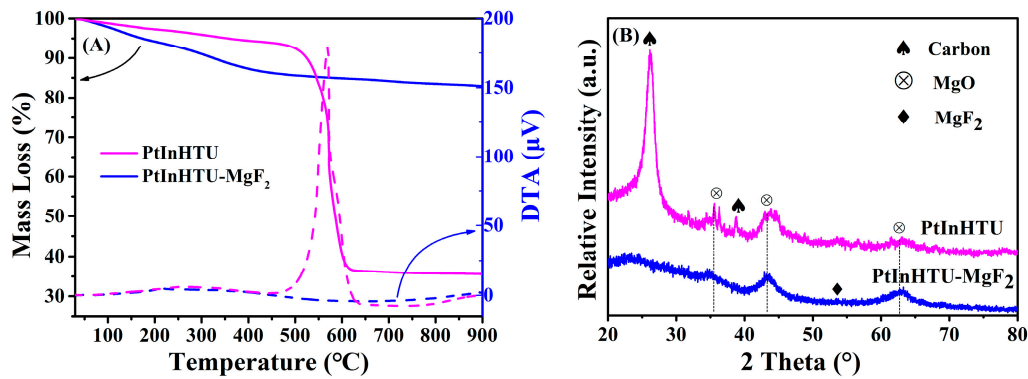


Figure 7. Thermogravimetric Analysis (TG-DTA) curves (A) and XRD patterns (B) of the spent catalysts.

### 2.3.2. SEM and TEM

The formation of coke deposits also can be confirmed by the SEM and TEM images of the spent catalysts (see Figure 8). Firstly, typical flake mesoporous materials can be kept for each spent catalyst, suggesting that there is no significant texture change for these catalysts after reaction. Additionally, more graphitized coke can be seen on the surface of PtInHTU. As expected, only the granular amorphous coke deposits can be seen on PtInHTU-MgF<sub>2</sub>, which is consistent with the TG results. By analyzing the particle size distribution of the spent catalysts, it can be found that the average diameters of PtInHTU and PtInHTU-MgF<sub>2</sub> has a slight increase from 1.3 to 2.7 nm and 1.2 to 2.1 nm, respectively. This demonstrates that the anti-sintering ability can be enhanced by introducing the MgF<sub>2</sub> species.

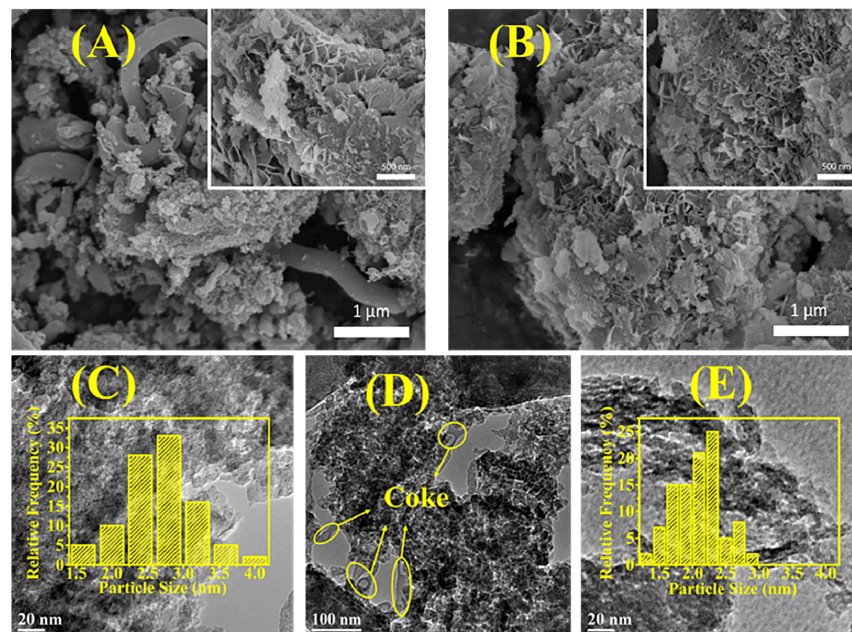


Figure 8. SEM images of spent catalysts: (A) PtInHTU, (B) PtInHTU-MgF<sub>2</sub>; TEM micrographs of spent catalysts (C,D) PtInHTU, (E) PtInHTU-MgF<sub>2</sub>.

### 3. Materials and Methods

#### 3.1. Materials Used

Mg(NO<sub>3</sub>)<sub>2</sub>·6H<sub>2</sub>O (Analytical grade chemicals, Fuchen Chemical Regents Factory, Tianjin, China), Al(NO<sub>3</sub>)<sub>3</sub>·9H<sub>2</sub>O (Analytical grade chemicals, Fuchen Chemical Regents Factory, Tianjin, China), urea (Analytical grade chemicals, Fuchen Chemical Regents Factory, Tianjin, China), SiO<sub>2</sub> (>98%, TANSAIL Advanced Materials Co. Ltd., Nanjing, China), KF (Analytical grade chemicals, Aladdin Industrial Corporation, Shanghai, China), H<sub>2</sub>PtCl<sub>6</sub>·6H<sub>2</sub>O (Analytical grade chemicals, Mascot Chemical Co. Ltd., Tianjin, China), In(NO<sub>3</sub>)<sub>3</sub>·xH<sub>2</sub>O (Analytical grade chemicals, Aladdin Industrial Corporation, Shanghai, China).

#### 3.2. Synthesis of Composites and Precursors

The HT-MgF<sub>2</sub> precursors were prepared by using the hydrothermal and alkali-etching method. Firstly, 0.2 g SiO<sub>2</sub>, 0.02 mol KF, 2.31 g Mg(NO<sub>3</sub>)<sub>2</sub>·6H<sub>2</sub>O, 1.69 g Al(NO<sub>3</sub>)<sub>3</sub>·9H<sub>2</sub>O, and 2.7 g urea were dissolved into 65 mL deionized water and stirred vigorously for 30 min. Then, the mixed solution was poured in a 100 mL Teflon autoclave and maintained at 100 °C for 20 h. The as-prepared product was filtered, washed with deionized water to neutrality, and dried in air at 100 °C overnight. Finally, 1 g the dried sample was put into 50 mL NaOH solution (1 mol·L<sup>-1</sup>) and stirred for 10 h. The resulting suspension was washed with deionized water to pH = 7, and the solid product was dried overnight at 100 °C. The obtained precursor was labeled as HT-MgF<sub>2</sub>.

The HT samples were prepared under same conditions, except without adding 0.02 mol KF into the initial solution. The corresponding precursor was named as HT.

#### 3.3. Synthesis of Catalysts

The calcined products were acquired by calcining at 600 °C for 4 h with a heating rate of 2 °C·min<sup>-1</sup>. The corresponding PtInHTC-MgF<sub>2</sub> catalyst was obtained via the stepwise incipient wetness impregnation method. Firstly, the In-based precursor was obtained by impregnating calcined HT-MgF<sub>2</sub> with In(NO<sub>3</sub>)<sub>3</sub>·xH<sub>2</sub>O aqueous solution at room temperature for 6 h and dried at 120 °C for 12 h. After that, the solid was calcined at 550 °C for 4 h. At the same time, the same procedure as In impregnation was conducted to introduce the Pt species using H<sub>2</sub>PtCl<sub>6</sub>·H<sub>2</sub>O as a precursor, except for an impregnation time of 2 h. The loading amount of Pt and In was 0.5 wt% and 1.4 wt%, respectively. After drying and calcination, the resulting solids were defined as PtInHTC-MgF<sub>2</sub>. PtInHTC was prepared in a same manner.

The calcined catalysts were reduced by 5 vol% H<sub>2</sub>/N<sub>2</sub> at a flow rate of 30 mL·min<sup>-1</sup> and 600 °C for 2 h with a heating rate of 5 °C·min<sup>-1</sup> to obtain the corresponding reduced catalysts, which were labeled as PtInHTR and PtInHTR-MgF<sub>2</sub>.

After the reaction of isobutane dehydrogenation to isobutene, the spent catalysts were marked as PtInHTU and PtInHTU-MgF<sub>2</sub>.

#### 3.4. Precursors, Composites and Catalysts Characterization

The XRD patterns of samples were collected on a Bruker D8-Focus X-ray diffractometer (Germany) equipped with a Cu K $\alpha$  radiation ( $\lambda = 0.15418$  nm).

Low-temperature N<sub>2</sub> adsorption–desorption tests were carried on a TriStar 3000 micromeritics apparatus (Micromeritics, Norcross, GA, USA).

The scanning electron microscopy (SEM) images were obtained using a MAIA3 TESAN.

The transmission electron microscopy (TEM) morphologies were observed on a JEM-2100F field-emission transmission electron microscope.

The temperature-programmed reduction (H<sub>2</sub>-TPR) was carried out by automatic multi-purpose adsorption apparatus (tp 5080 XQINSTRUMENT CO., Tianjin, China).

The X-ray photoelectron spectra (XPS) of catalysts were tested on a Thermo ESCALAB 250Xi (US) using Al K $\alpha$  radiation.

Thermogravimetric analysis (TG-DTA) was carried out on a DTG-50/50H (PerkinElmer, Waltham, MA, USA).

### 3.5. Catalytic Dehydrogenation Performance Test

The isobutane dehydrogenation to isobutene reactions were performed in a fixed-bed continuous-flow reactor at 600 °C under atmospheric pressure. The calcined catalyst (0.5 g, 40–60 mesh) was placed into the reactor and reduced at 600 °C for 2 h with a heating rate of 5 °C·min<sup>-1</sup> in 5 vol% H<sub>2</sub>/N<sub>2</sub>. After reduction, the isobutane and hydrogen (the molar ratio of iC<sub>4</sub>H<sub>10</sub>:H<sub>2</sub> = 1:1) were introduced into the reactor, in which the weight hourly space velocity (WHSV) of isobutane was 3 h<sup>-1</sup>. The reactions were performed at 600 °C, and an online gas chromatograph (GC) equipped with a flame ionization detector (Al<sub>2</sub>O<sub>3</sub> packed column) was employed to analyze the gaseous products.

## 4. Conclusions

In summary, the MgF<sub>2</sub>-modified hydrotalcite-derived composites supported Pt-In catalyst PtInHTR-MgF<sub>2</sub> can be synthesized by a combination of the hydrothermal method, alkali-etching, and impregnation strategy. The formation of MgF<sub>2</sub> can not only construct the special texture and morphology of catalyst, but also disperse the active metals, inhibit the reduction of the In<sup>3+</sup> species, and adjust the acidity of the catalyst. These features can improve the activity and selectivity of isobutane direct dehydrogenation and make the catalyst obtain a high durability and excellent resistance to coking and sintering.

**Author Contributions:** Conceptualization, Z.S. and J.W.; methodology and experiments, Z.S. and J.W.; Statistics and data validation, Z.S. and É.M.; writing—original draft preparation, Z.S.; writing—review and editing, F.L. and X.Z.; research ideas, analyzed data, revised the manuscript and funding acquisition, L.Z. All authors have read and agreed to the published version of the manuscript.

**Funding:** This research was funded by the National Natural Science Foundation of China (21776214).

**Institutional Review Board Statement:** Not applicable.

**Informed Consent Statement:** Not applicable.

**Data Availability Statement:** Data is contained within the article.

**Conflicts of Interest:** The authors declare no conflict of interest.

## References

1. Zhu, G.; Li, P.; Zhao, F.; Song, H.; Xia, C. Selective aromatization of biomass derived diisobutylene to p-xylene over supported non-noble metal catalysts. *Catal. Today* **2016**, *276*, 105–111. [[CrossRef](#)]
2. Sharma, R.K.; Mohanty, S.; Gupta, V. Advances in butyl rubber synthesis via cationic polymerization: An overview. *Polym. Int.* **2021**. [[CrossRef](#)]
3. Chen, C.; Zhang, S.M.; Wang, Z.; Yuan, Z.Y. Ultrasmall Co confined in the silanols of dealuminated beta zeolite: A highly active and selective catalyst for direct dehydrogenation of propane to propylene. *J. Catal.* **2020**, *383*, 77–87. [[CrossRef](#)]
4. Chen, C.; Sun, M.L.; Hu, Z.P.; Ren, J.T.; Zhang, S.M.; Yuan, Z.Y. New insight into the enhanced catalytic performance of ZnPt/HZSM-5 catalysts for direct dehydrogenation of propane to propylene. *Catal. Sci. Technol.* **2019**, *9*, 1979–1988. [[CrossRef](#)]
5. Hill, J.M.; Cortright, R.D.; Dumesic, J.A. Silica- and L-zeolite-supported Pt, Pt/Sn and Pt/Sn/K catalysts for isobutane dehydrogenation. *Appl. Catal. A* **1998**, *168*, 9–21. [[CrossRef](#)]
6. Ohta, M.; Ikeda, Y.; Igarashi, A. Additive effect on properties of Pt/ZnO catalyst for dehydrogenation of isobutane at low temperatures. *J. Jpn. Petrol. Inst.* **2002**, *45*, 150–155. [[CrossRef](#)]
7. Miura, H.; Itoh, T. Selective deposition of Sn on the Pt surface of Pt/ZnAl<sub>2</sub>O<sub>4</sub> catalyst and addition effect on isobutane dehydrogenation. *React. Kinet. Catal. Lett.* **1999**, *66*, 189–194. [[CrossRef](#)]
8. Rashidi, M.; Nikazar, M.; Rahmani, M.; Mohamadghasemi, Z. Kinetic modeling of simultaneous dehydrogenation of propane and isobutane on Pt-Sn-K/Al<sub>2</sub>O<sub>3</sub> catalyst. *Chem. Eng. Res. Des.* **2015**, *95*, 239–247. [[CrossRef](#)]
9. Zangeneh, F.T.; Sahebdehfar, S.; Bahmani, M. Propane Dehydrogenation over a Commercial Pt-Sn/Al<sub>2</sub>O<sub>3</sub> Catalyst for Isobutane Dehydrogenation: Optimization of Reaction Conditions. *Chin. J. Chem. Eng.* **2013**, *21*, 730–735. [[CrossRef](#)]
10. Tolek, W.; Suriye, K.; Praserthdam, P.; Panpranot, J. Enhanced stability and propene yield in propane dehydrogenation on PtIn/Mg(Al)O catalysts with various In loadings. *Top. Catal.* **2018**, *61*, 1624–1632. [[CrossRef](#)]
11. Li, J.; Zhang, M.; Song, Z.; Liu, S.; Wang, J.; Zhang, L. Hierarchical PtIn/Mg(Al)O derived from reconstructed PtIn-hydrotalcite-like compounds for highly efficient propane dehydrogenation. *Catalysts* **2019**, *9*, 767. [[CrossRef](#)]
12. Xia, K.; Lang, W.; Li, P.; Long, L.; Yan, X.; Guo, Y. The influences of Mg/Al molar ratio on the properties of PtIn/Mg(Al)O-x catalysts for propane dehydrogenation reaction. *Chem. Eng. J.* **2016**, *284*, 1068–1079. [[CrossRef](#)]

13. Xia, K.; Lang, W.; Li, P.; Yan, X.; Guo, Y. The properties and catalytic performance of PtIn/Mg(Al)O catalysts for the propane dehydrogenation reaction: Effects of pH value in preparing Mg(Al)O supports by the co-precipitation method. *J. Catal.* **2016**, *338*, 104–114. [[CrossRef](#)]
14. Ma, Z.; Wu, Z.; Miller, J.T. Effect of Cu content on the bimetallic Pt-Cu catalysts for propane dehydrogenation. *Catal. Struct. React.* **2017**, *3*, 43–53. [[CrossRef](#)]
15. Liu, Y.; Xia, C.; Wang, Q.; Zhang, L.; Huang, A.; Ke, M.; Song, Z. Direct dehydrogenation of isobutane to isobutene over Zn-doped ZrO<sub>2</sub> metal oxide heterogeneous catalysts. *Catal. Sci. Technol.* **2018**, *8*, 4916–4924. [[CrossRef](#)]
16. Silvestre-Albero, J.; Sanchez-Castillo, M.A.; He, R.; Sepulveda-Escribano, A.; Rodriguez-Reinoso, F.; Dumesic, J.A. Microcalorimetric, reaction kinetics and DFT studies of Pt-Zn/X-zeolite for isobutane dehydrogenation. *Catal. Lett.* **2001**, *74*, 17–25. [[CrossRef](#)]
17. Siddiqi, G.; Sun, P.; Galvita, V.; Bell, A.T. Catalyst performance of novel Pt/Mg(Ga)(Al)O catalysts for alkane dehydrogenation. *J. Catal.* **2010**, *274*, 200–206. [[CrossRef](#)]
18. Wang, T.; Jiang, F.; Liu, G.; Zeng, L.; Zhao, Z.J.; Gong, J.L. Effects of Ga doping on Pt/CeO<sub>2</sub>-Al<sub>2</sub>O<sub>3</sub> catalysts for propane dehydrogenation. *AIChE J.* **2016**, *62*, 4365–4376. [[CrossRef](#)]
19. Yang, K.; Yin, Y.; Lai, S.; Zhu, L.; Zhang, J.; Lai, W.; Lian, Y.; Fang, W. Aromatization of n-Butane and i-Butane over PtSnK/ZSM-5 Catalysts: Influence of SiO<sub>2</sub>/Al<sub>2</sub>O<sub>3</sub> Ratio. *Catal. Lett.* **2018**, *148*, 3570–3582. [[CrossRef](#)]
20. Li, Q.; Yang, G.B.; Wang, K.; Wang, X.T. Preparation of carbon-doped alumina beads and their application as the supports of Pt-Sn-K catalysts for the dehydrogenation of propane. *React. Kinet. Mech. Catal.* **2020**, *129*, 805–817. [[CrossRef](#)]
21. Ballarini, A.D.; de Miguel, S.R.; Castro, A.A.; Scelza, O.A. n-Decane dehydrogenation on Pt, PtSn and PtGe supported on spinels prepared by different methods of synthesis. *Appl. Catal. A* **2013**, *467*, 235–245. [[CrossRef](#)]
22. Rimaz, S.; Chen, L.W.; Kawi, S.; Borgna, A. Promoting effect of Ge on Pt-based catalysts for dehydrogenation of propane to propylene. *Appl. Catal. A* **2019**, *588*, 117266. [[CrossRef](#)]
23. Ji, Z.H.; Miao, D.Y.; Gao, L.J.; Pan, X.L.; Bao, X.H. Effect of pH on the catalytic performance of PtSn/B-ZrO<sub>2</sub> in propane dehydrogenation. *Chin. J. Catal.* **2020**, *41*, 719–729. [[CrossRef](#)]
24. Wu, G.; Wang, X.; Wei, W.; Sun, Y. Fluorine-modified Mg-Al mixed oxides: A solid base with variable basic sites and tunable basicity. *Appl. Catal. A* **2010**, *377*, 107–113. [[CrossRef](#)]
25. Wu, G.; Wang, X.; Chen, B.; Li, J.; Zhao, N.; Wei, W.; Sun, Y. Fluorine-modified mesoporous Mg-Al mixed oxides: Mild and stable base catalysts for O-methylation of phenol with dimethyl carbonate. *Appl. Catal. A* **2007**, *329*, 106–111. [[CrossRef](#)]
26. Liu, J.; Liu, C.; Ma, A.; Rong, J.; Da, Z.; Zheng, A.; Qin, L. Effects of Al<sub>2</sub>O<sub>3</sub> phase and Cl component on dehydrogenation of propane. *Appl. Surf. Sci.* **2016**, *368*, 233–240. [[CrossRef](#)]
27. Zhu, Q.; Zhang, H.; Zhang, S.; Wang, G.; Zhu, X.; Li, C. Dehydrogenation of isobutane over a Ni-P/SiO<sub>2</sub> catalyst: Effect of P addition. *Ind. Eng. Chem. Res.* **2019**, *58*, 7834–7843. [[CrossRef](#)]
28. Matveyeva, A.N.; Wärnå, J.; Pakhomov, N.A.; Murzin, D.Y. Kinetic modeling of isobutane dehydrogenation over Ga<sub>2</sub>O<sub>3</sub>/Al<sub>2</sub>O<sub>3</sub> catalyst. *Chem. Eng. J.* **2020**, *381*, 122741. [[CrossRef](#)]
29. Dong, A.H.; Wang, K.; Zhu, S.Z.; Yang, G.B.; Wang, X.T. Facile preparation of PtSn-La/Al<sub>2</sub>O<sub>3</sub> catalyst with large pore size and its improved catalytic performance for isobutane dehydrogenation. *Fuel Process. Technol.* **2017**, *158*, 218–225. [[CrossRef](#)]
30. Sun, G.; Huang, Q.; Li, H.; Liu, H.; Zhang, Z.; Wang, X.; Wang, Q.; Wang, J. Different supports-supported Cr-based catalysts for oxidative dehydrogenation of isobutane with CO<sub>2</sub>. *Chin. J. Catal.* **2014**, *32*, 1424–1429. [[CrossRef](#)]
31. Deng, L.D.; Zhou, Z.J.; Shishido, T. Behavior of active species on Pt-Sn/SiO<sub>2</sub> catalyst during the dehydrogenation of propane and regeneration. *Appl. Catal. A* **2020**, *606*, 117826. [[CrossRef](#)]
32. Otroshchenko, T.P.; Kondratenko, V.A.; Rodemerck, U.; Linke, D.; Kondratenko, E.V. Non-oxidative dehydrogenation of propane, n-butane, and isobutane over bulk ZrO<sub>2</sub>-based catalysts: Effect of dopant on the active site and pathways of product formation. *Catal. Sci. Technol.* **2017**, *7*, 4499–4510. [[CrossRef](#)]
33. Liu, J.; Zhou, W.; Jiang, D.; Wu, W.; Miao, C.; Wang, Y.; Ma, X. Isobutane dehydrogenation over InPtSn/ZnAl<sub>2</sub>O<sub>4</sub> catalysts: Effect of indium promoter. *Ind. Eng. Chem. Res.* **2018**, *57*, 11265–11270. [[CrossRef](#)]
34. Vu, B.K.; Song, M.B.; Ahn, I.Y.; Suh, Y.W.; Suh, D.J.; Kim, W.I.; Koh, H.L.; Choi, Y.G.; Shin, E.W. Pt-Sn alloy phases and coke mobility over Pt-Sn/Al<sub>2</sub>O<sub>3</sub> and Pt-Sn/ZnAl<sub>2</sub>O<sub>4</sub> catalysts for propane dehydrogenation. *Appl. Catal. A* **2011**, *400*, 25–33. [[CrossRef](#)]
35. Zhang, M.; Song, Z.; Guo, M.Q.; Li, X.X.; Lin, Y.J.; Zhang, L.H. Effect of reduction atmosphere on structure and catalytic performance of PtIn/Mg(Al)O/ZnO for propane dehydrogenation. *Catalysts* **2020**, *10*, 485. [[CrossRef](#)]
36. Wu, P.; Xia, L.; Liu, Y.; Wu, J.S.; Chen, Q.Y.; Song, S.X. Simultaneous sorption of arsenate and fluoride on calcined Mg-Fe-La hydrotalcite-like compound from water. *ACS Sustain. Chem. Eng.* **2018**, *6*, 16287–16297. [[CrossRef](#)]
37. Mimura, N.; Takahara, I.; Saito, M.; Sasaki, Y.; Murata, K. Dehydrogenation of ethylbenzene to styrene in the presence of CO<sub>2</sub> over calcined hydrotalcite-like compounds as catalysts. *Catal. Lett.* **2002**, *78*, 125–128. [[CrossRef](#)]
38. Sun, P.; Siddiqi, G.; Vining, W.C.; Chi, M.; Bell, A.T. Novel Pt/Mg(In)(Al)O catalysts for ethane and propane dehydrogenation. *J. Catal.* **2011**, *282*, 165–174. [[CrossRef](#)]
39. Yang, X.; Liu, G.; Li, Y.; Zhang, L.; Wang, X.; Liu, Y. Novel Pt-Ni bimetallic catalysts Pt(Ni)-LaFeO<sub>3</sub>/SiO<sub>2</sub> via lattice atomic-confined reduction for highly efficient isobutane dehydrogenation. *Trans. Tianjin Univ.* **2018**, *25*, 245–257. [[CrossRef](#)]
40. Wang, Q.; Wang, X.; Xu, J.; Ouyang, X.; Hou, X.; Chen, D.; Wang, R.; Shen, G. Flexible coaxial-type fiber supercapacitor based on NiCo<sub>2</sub>O<sub>4</sub> nanosheets electrodes. *Nano Energy* **2014**, *8*, 44–51. [[CrossRef](#)]

41. Liu, Y.; Li, Y.; Ge, M.; Chen, X.; Guo, M.; Zhang, L. Perovskite-derived Pt-Ni/Zn(Ni)TiO<sub>3</sub>/SiO<sub>2</sub> catalyst for propane dehydrogenation to propene. *Catal. Lett.* **2019**, *149*, 2552–2562. [[CrossRef](#)]
42. Passos, F.B.; Aranda, D.A.G.; Schmal, M. Characterization and catalytic activity of bimetallic Pt-In/Al<sub>2</sub>O<sub>3</sub> and Pt-Sn/Al<sub>2</sub>O<sub>3</sub> catalysts. *J. Catal.* **1998**, *178*, 478–488. [[CrossRef](#)]
43. Marchesini, F.A.; Gutierrez, L.B.; Querini, C.A.; Miro, E.E. Pt, In and Pd, In catalysts for the hydrogenation of nitrates and nitrites in water. FTIR characterization and reaction studies. *Chem. Eng. J.* **2010**, *159*, 203–211. [[CrossRef](#)]
44. Im, J.; Choi, M. Physicochemical stabilization of Pt against sintering for a dehydrogenation catalyst with high activity, selectivity, and durability. *ACS Catal.* **2016**, *6*, 2819–2826. [[CrossRef](#)]
45. Xia, K.; Lang, W.; Li, P.; Yan, X.; Guo, Y. Analysis of the catalytic activity induction and deactivation of PtIn/Mg(Al)O catalysts for propane dehydrogenation reaction. *RSC Adv.* **2015**, *5*, 64689–64695. [[CrossRef](#)]
46. Chen, H.; Jie, Y.; Chang, L.; Chen, X. Reaction behavior of MgF<sub>2</sub> powder in hexafluoropropylene/air atmospheres at high temperatures. *Solid State Ion.* **2019**, *340*, 115016. [[CrossRef](#)]
47. Han, W.; Zhang, C.; Wang, H.; Zhou, S.; Tang, H.; Yang, L.; Wang, Z. Sub-nano MgF<sub>2</sub> embedded in carbon nanofibers and electrospun MgF<sub>2</sub> nanofibers by one-step electrospinning as highly efficient catalysts for 1,1,1-trifluoroethane dehydrofluorination. *Catal. Sci. Technol.* **2017**, *7*, 6000–6012. [[CrossRef](#)]
48. Chen, X.; Ge, M.; Li, Y.; Liu, Y.; Wang, J.; Zhang, L. Fabrication of highly dispersed Pt-based catalysts on  $\gamma$ -Al<sub>2</sub>O<sub>3</sub> supported perovskite Nano islands: High durability and tolerance to coke deposition in propane dehydrogenation. *Appl. Surf. Sci.* **2019**, *490*, 611–621. [[CrossRef](#)]
49. Zhao, S.Y.; Xu, B.L.; Yu, L.; Fan, Y.N. Catalytic dehydrogenation of propane to propylene over highly active PtSnNa/ $\gamma$ -Al<sub>2</sub>O<sub>3</sub> catalyst. *Chin. Chem. Lett.* **2018**, *29*, 475–478. [[CrossRef](#)]
50. Zhang, Y.; Zhou, Y.; Wan, L.; Xue, M.; Duan, Y.; Liu, X. Effect of magnesium addition on catalytic performance of PtSnK/ $\gamma$ -Al<sub>2</sub>O<sub>3</sub> catalyst for isobutane dehydrogenation. *Fuel Process. Technol.* **2011**, *92*, 1632–1638. [[CrossRef](#)]
51. Zhang, Y.; Zhou, Y.; Shi, J.; Sheng, X.; Duan, Y.; Zhou, S.; Zhang, Z. Effect of zinc addition on catalytic properties of PtSnK/ $\gamma$ -Al<sub>2</sub>O<sub>3</sub> catalyst for isobutane dehydrogenation. *Fuel Process. Technol.* **2012**, *96*, 220–227. [[CrossRef](#)]
52. Vaezifar, S.; Faghihian, H.; Kamali, M. Dehydrogenation of isobutane over Sn/Pt/Na-ZSM-5 catalysts: The effect of SiO<sub>2</sub>/Al<sub>2</sub>O<sub>3</sub> ratio, amount and distribution of Pt nanoparticles on the catalytic behavior. *Korean J. Chem. Eng.* **2010**, *28*, 370–377. [[CrossRef](#)]
53. Li, B.; Xu, Z.; Jing, F.; Luo, S.; Chu, W. Facile one-pot synthesized ordered mesoporous Mg-SBA-15 supported PtSn catalysts for propane dehydrogenation. *Appl. Catal. A* **2017**, *533*, 17–27. [[CrossRef](#)]